

1 Introduction

Submarine permafrost refers to solid earth material below modern sea level that has perennial temperatures below 0 °C. It contains and traps significant amounts of methane and organic carbon, which may be released to the atmosphere during permafrost warming and thawing (McGuire et al., 2009), if not oxidized before it reaches the seabed (Overduin et al., 2015). Cold sediment temperatures stabilized by shelf permafrost extend the gas-hydrate stability zone (Dallimore and Collett, 1995) and the frozen sediment may limit gas diffusion into the water column and atmosphere (Shakhova and Semiletov, 2007). Despite its importance, little of what we know about submarine permafrost distribution and temperature is based on direct observation, especially on the East Siberian shelves, which make up over 80 % of the potentially permafrost-affected arctic shelf area (Brown et al., 2001).

Most submarine permafrost originally formed as terrestrial permafrost on arctic shelves, exposed during late Pleistocene cold periods, which was subsequently inundated by rising sea levels following the last glacial period. Even today, rapid coastal retreat along the ice-rich coastline of the Laptev and East Siberian shelf seas causes about 10 km² of land loss annually (Grigoriev, 2008). Deglaciation after the Last Glacial Maximum led to sea-level rise in the Laptev Sea region more than ten times as rapid as modern rates (Bauch et al., 2001), inundating most of the more than 1.5 million km² East Siberian shelf region within several thousand years. Both processes (coastal erosion and sea-level rise) covered cold (less than -2 °C at the seasonal damping depth) and thick (hundreds of meters) permafrost with sea water and seasonal sea ice, separating it from the cold air with mean annual temperatures of less than -10 °C. In the coastal zone (shallower than 10 m) of the Laptev Sea, bottom temperatures currently range from 1.6 °C in summer to -1.4 °C in winter (Dmitrenko et al., 2011). After inundation, submarine permafrost began to equilibrate thermally with benthic temperatures. This temperature increase results in warming and thawing of permafrost below the seabed (Lachenbruch, 1957). Thawing also occurred due to penetration of salt-water into

3743

the sea-bed, which lowered the freezing point of the sediment's pore water. Thus, modern submarine permafrost can have temperatures below 0 °C but contain little or no ice. What is generally observed, by geophysical methods or direct observation in sediment cores, is the depth of ice-bonded permafrost (IBP) below the sea floor (which is equivalent to the thickness of the overlying unfrozen sediment). Direct current resistivity and controlled source electromagnetic techniques for the investigation of submarine permafrost have been established in a number of studies (Barnes, 1963; Constable, 2010; Corwin, 1983; Sellmann et al., 1989). Laboratory measurements of the bulk electrical properties of frozen porous media show the effect of ice content and thus saline pore water on electrical resistivity (Overduin et al., 2012). Sediment bulk electrical resistivity increases by orders of magnitude between ice-bonded, freshwater sediment and ice-free, saline sediment (Scott et al., 1990), making it suitable for the detection of the ice-bonded permafrost table.

Benthic temperature and salinity control warming of the sea floor and the rate of salt penetration into the sediment column, but there are number of processes active in shallow water near the coastline that additionally affect permafrost following inundation. Sedimentation of eroded material, sediment re-suspension and transport by wave action and by currents and the entrainment of suspended material and sediment in sea ice are important in determining initial rates of degradation in water depths where wave cycles and ice gouging can turbate and erode the sea bed. Where the water depth is less than the maximum sea ice thickness, bottom-fast ice (BFI) forms (Solomon et al., 2008). Sea ice has a higher thermal conductivity than sea water, and BFI thermally couples the sea floor to the cold winter air temperatures, which can lead to seasonal freezing of the sediment and the injection of brines into the sediment (Harrison, 1982). Since the rate of coastal erosion affects sediment flux, and therefore bathymetry, submarine permafrost degradation rates following inundation are probably related to coastal erosion.

3744

Our objective is to use inundation periods inferred from remote sensing, geophysical surveys and borehole observations of IBP to investigate the relationship between coastal erosion and submarine permafrost degradation beneath the shoreface

2 Study area

5 Muostakh Island (71.58° N, 130.01° E), a sliver of land about 40 km offshore of Tiksi in the central Laptev Sea (Fig. 1), is an ideal site for the study of submarine permafrost processes (Are, 2003). About 10 km long and less than 500 m wide, the island is located 25 km north-east of the mainland and 15 km south-east of Bykovsky Peninsula. Ships leaving Tiksi, one of the major ports on the Northeast Passage, travel within sight
10 of Muostakh Island, and it has therefore long been an object of research, from as early as the late 19th century. This research includes studies of coastal dynamics, and coastline erosion rates observed at Muostakh Island in the central Laptev Sea include some of the highest observed in the Arctic (Grigoriev et al., 2009). The island was originally the south-eastern continuation of the Bykovsky Peninsula coast and consists mainly of
15 late Pleistocene Ice Complex (IC) deposits. IC deposits are ice-rich (Muostakh Island is composed of 87 % ground ice by volume; Günther et al., 2015), polygenetic in origin, and characterized at the ground surface by the polygonal network of ice wedges formed over thousands of years by melt-water infiltration into cold winter thermal contraction cracks (Schirrmeyer et al., 2011b). Coastal thermo-erosion on Muostakh Island varies
20 widely in intensity (from close to 0 to over 25 m a⁻¹) over a relatively small region (Grigoriev et al., 2009; Günther et al., 2015). The spatial variability of coastal retreat rates along the island's coastline offers an opportunity to investigate its influence on submarine permafrost development while other aspects of environmental forcing are similar.

IC coastlines are prevalent throughout much of the Laptev and East Siberian seas.
25 On Muostakh Island, IC deposits are exposed along the east coast from below sea level up to the island's surface. Much of the Chukchi and Beaufort seas coastlines are similarly ice-rich and can be expected to be subject to the same mechanisms of geo-

3745

morphologic change in response to shifts in environmental drivers of coastal dynamics (Ping et al., 2011). Regionally, relevant shifts in the energy and water balances at the land-atmosphere interface (Boike et al., 2013), increases in Lena River discharge (Fedorova et al., 2015), and increases in the duration of open water and coastal erosion
5 (Günther et al., 2015) have been recently observed, matching similar circumpolar observations (Barnhart et al., 2014).

3 Materials and methods

3.1 Geodetic measurements of coastline position

Coastal change rates on Muostakh Island have been estimated since the early 1950s
10 by combining on-site and remote sensing methods (Fig. 2; Grigoriev et al., 2009). A geodetic benchmark was established near the northern end of the island in 1950. Measurements were made at irregular intervals thereafter, by measuring the distance from the geodetic benchmark to the top of the coastal bluff along various bearings, either with measuring tape or a theodolite. The coastline positions reported here were
15 measured as the position of the upper edge of the coastal bluff along a bearing from the geodetic benchmark and the signal tower on Cape Muostakh, at the southern end of the Bykovsky Peninsula. Since there were unrecorded differences from year to year in how measurements were carried out, it is difficult to assess uncertainty in the measurements. Sources of uncertainty include determination of the direction in which coastal
20 position was measured, small differences in time of year for measurements, and difficulty in safely reaching the cliff edge. We conservatively estimate the measurements to be better than ±0.5 m. Between measurements in 2010 and 2011, the geodetic reference point was toppled by coastal erosion. For purposes of continuity, a network of survey points was established by theodolite in 2011 immediately thereafter to make
25 a continuation of the measurement series possible. Ground control points were established to align field observations with remote sensing data (Günther et al., 2013).

3746

3.2 Temperature and electrical resistivity

Benthic temperature and electrical conductivity were recorded using a bottom-moored conductivity ($\pm 0.1 \text{ mS cm}^{-1}$), temperature ($\pm 0.2 \text{ }^\circ\text{C}$) and water depth ($\pm 0.2 \%$) (CTD) datalogger. The CTD datalogger (Minilogger, UIT Umwelttechnik GmbH) was mounted on a metal plate and deployed with two 50 m cables attached to anchors. By dredging with a cat's claw anchor after deployment, the cables could be snagged and the datalogger recovered. The datalogger was deployed at 71.672° N , 129.996° E in 7.2 m water depth on 10 August 2008, just outside of the north-eastern corner of the frame for Fig. 1b. Data were collected hourly between 1 September 2008 and 31 August 2009. Although electrical conductivity values were measured and recorded, the inverse value (electrical resistivity) is reported here for comparison to the results of the geoelectrical surveys.

3.3 Core and borehole data

Sediments of on-shore and off-shore permafrost north of Muostakh Island were drilled during the Northern Expedition of the Siberian Branch of the Soviet Academy of Sciences (SBSAS) Permafrost Institute Yakutsk in 1982 and 1983. Six boreholes were sunk up to 54 m depth and 2.5 km off the shore (in 1983) along a straight line across the shallow water zone between Cape Muostakh at the southern end of the Bykovsky Peninsula and the northern cape of Muostakh Island (Kunitsky, 1989; Slagoda, 2004). The boreholes were drilled using a portable rotary drill rig and a dry drilling technique. Metal casing was drilled through the sea ice, water column and into the sediment to prevent water from entering the borehole. Temperature and geochemical data are summarized by Kunitsky (1989) while granulometric, cryolithologic and mineralogic data are presented by Slagoda (1993, 2004). Results from these publications, originally in Russian, are made available here to a non-Russian readership. Observations made during drilling from the land-fast ice in spring and during laboratory investigation of the cores included sediment temperature and lithology, and pore-water salinity. Borehole tem-

3747

peratures were measured in 1982 and 1983 using a thermistor string and a voltmeter. Sediment porewater from cores was analyzed for total dissolved solids, which was converted to electrical resistivity based on the resistivity of a sodium chloride solution:

$$R = 0.55 \cdot \text{TDS} - 0.97 \quad (1)$$

where R is the electrical resistivity in Ωm and TDS are the total dissolved solids in g per 100 g solution. Locations of boreholes, their depths, water depth and the depth of the unfrozen/frozen interface beneath sea level are summarized in Table 1.

3.4 Electrical resistivity and inundation derivation

Geoelectric surveys of submarine apparent resistivity collected on 21–24 August 2011 were combined with bathymetry measurements to invert for sub-bottom sediment resistivity, which gives an indication of the depths of saline sediment and of the underlying ice-bonded submarine permafrost. The results from three surveys are presented here, two profiles of 1.5 km length from the eastern and western coasts of the northern cape of Muostakh Island, as well as a profile of 4 km length along the historical borehole profile (Fig. 1). The sub-bottom apparent electrical resistivity profiles were collected using an IRIS Syscal Pro™ Deep Marine system. Voltages were measured around an electrical current injection dipole of 10 m size, using a floating electrode streamer towed behind a small boat. The injection and potential electrodes were stainless steel plates (10 cm \times 30 cm). Electrical potential was measured across 10 channels spanning between 20 and 110 m. Electrode position (relative to a GPS aboard the boat), the injection current, measured electrode pair potentials and water depth (using an echo-sounder with better than $\pm 0.1 \text{ m}$ resolution attached to the boat) were recorded at intervals of at least 2 m as the array was towed. We used RES2DINV™ software to invert the apparent resistivity data via least-squares inversion for floating electrodes with a modelled water-layer resistivity, allowing for a sharp change in modelled resistivity across sediment surface. Model resistivity was smoothed to produce reasonable variations in the resistivity values. Prior to inversions, data values were inspected graphi-

3748

cally and less than 0.1 % of collected apparent resistivities were identified as outliers and removed. Inversions required less than 5 iterations in order to reach better than 5 % RMS error between modelled and observed resistivity. Kang and Lee (2015) show an increase in electrical resistivity on freezing for silt-sand mixtures with 40 % saturation from around 100 Ω m to over 300 k Ω m. For 100 % saturated mixtures with saline pore water, the resistivities can be expected to be around 4 to 10 times lower (Kang and Lee, 2015). Laboratory measurements of saline silt and sand sediment show that ice is present in the sediment for bulk resistivities over 10 Ω m (Overduin et al., 2012). IBP depth was defined at values of 15 Ω m and higher. This assumption is based on laboratory measurements of bulk resistivity as a function of temperature and salinity for marine sediments which show that the change in bulk sediment resistivity from an unfrozen seawater-saturated sediment to a frozen ice-saturated sediment corresponds to a jump in resistivity from less than 10 to over 100 Ω m (Frolov, 1998; King et al., 1988; Overduin et al., 2012). Uncertainties in IBP depth estimated from resistivity profiles correspond to the depth range of the bulk sediment resistivity increase from 10 to 20 Ω m.

To determine mean submarine permafrost degradation rate, the depth to IBP (z_{pf}) and the time of erosion (t_0 ; time of inundation) were determined. z_{pf} was either determined by direct observation from historic borehole data, or was based on geoelectric survey inversions. The time since inundation was determined using coastlines digitized from remotely sensed imagery. In addition to the remote sensing dataset used by Günther et al. (2015), we increased temporal resolution by adding coastal erosion observations based on a CORONA KH-4B satellite image dating from 24 July in 1969, a HEXAGON image from 17 July 1975, and a SPOT-4 image taken on 1 July 2001. After stitching image tiles of the CORONA and HEXAGON images and pansharpener of the SPOT scene, each image was orthorectified to mean sea level using specific sensor models. In contrast to on-site measurements of the upper coastal bluff edge, we digitized the cliff bottom line as the location where inundation occurs in the form of thermo-abrasion (Are, 1988). For consistency with the 1983 drilling campaign, as an

3749

important baseline, the coastline of 1983 was reconstructed based on an interpolation between digitized coastlines from high resolution aerial and satellite images (1951, 1964, 1969, 1975, 2001, 2010 and 2011). Taking digitized coastlines as isolines of equal time, we estimated the time of inundation (t_0) at the location of each sounding in 2011. Given a mean coastal erosion rate of 1.8 m a^{-1} on Muostakh (Günther et al., 2015), interpolation was done to a raster size of 2 m, corresponding to a resolution of at least 1 year. However, our geoelectric transects are concentrated around the northern cape, where more rapid erosion is taking place, resulting in an almost monthly resolution. For two of the transects, some of the geoelectric measurement sites lay within the region flooded by sea water since 1951 (83 soundings from the borehole profile and 337 from the eastern transects). We calculated the period of inundation (t_{sub}) at the location of each sounding as:

$$t_{sub} = t_{obs} - t_0 \quad (2)$$

where t_{obs} is the time of observation (2011) and t_0 the time of inundation raster cell value. This yields a mean rate of submarine permafrost degradation for this period of:

$$r_{deg} = \frac{z_{pf}}{t_{sub}} \quad (3)$$

Variations of coastal erosion rate on shorter time scales (the longest averaging period was 26 years between 1975 and 2001) may occur but cannot be captured at this temporal resolution. Nautical charts of the early 1980s showing points of bathymetry measurements every 500 m and isobaths with an equidistance of 2 m were digitized and interpolated for the coastal waters around Muostakh, in order to account for shoreface profile changes.

3750

4 Results

4.1 Shoreface morphology

Figure 1 shows coastlines of Muostakh Island from two different points in time. Based on data from Grigoriev et al. (2009), the mean erosion rates for the northern cape of Muostakh Island for the period of record (1951–2014) was 10.7 m a^{-1} with variations between 2 and 25 m a^{-1} (Fig. 2). This value includes multiple-year periods for which erosion rate was determined using remote sensing data. Observations between 1995 and 2014 were conducted in the field, and give a mean erosion rate of 10.2 m a^{-1} . Longer-term coastal erosion rates of over 10 m a^{-1} decreased to less than 5 m a^{-1} in 1984 and then fluctuated between 2 and 10 m a^{-1} until 2006. In 2006/07, rates at the northern cape increased to 25 m a^{-1} . The three periods with the most rapid rates were observed in the past nine years (2006–2007, 2007–2009, 2010–2011). Rates of coastal retreat along the eastern shore of the island reported by Günther et al. (2015) confirm recent higher rates of erosion relative to the long-term means. In that context, the rates shown here are more indicative of the increased rates of land loss at the exposed cape than of changes in erosion rates for the island as a whole. For example, the western coast of Muostakh Island has had mean coastal erosion rates of less than 1 m a^{-1} (Fig. 1) for the past 60 years. The mean annual rates of erosion where the digitized coastlines intersected with the geoelectric profiles on the western and northeastern sides of the island over the period 1982–2011 were 0.5 and 6.5 m a^{-1} , respectively, resulting in the inundation of 14 m (western shore) and over 180 m (eastern shore) of land over this period.

Based on positions reported in the field notes of the drilling campaigns (Kunitsky, 1989) core positions were charted and used to define the position of the northwestern geoelectrical resistivity profile (Drilling profile in Fig. 1). Due to coastline retreat, the southern 1.4 km of this resistivity profile corresponded to what had been land at the time of coring in 1983, 645 m of which were within the drilling profile (Fig. 1). The altitude of the coastal bluff in 1983 exceeded 20 m a.s.l. (Fig. 3). Bathymetric profiling

3751

was used to survey modern water depths and comparisons showed that shoreward of 2 km in the historical data (Fig. 3), coastal retreat resulted in the erosion of the coastal bluff and eroded the shoreface profile, increasing water depths by up to 3 m. Changes in bathymetric profile over 30 years from about 1.8 km out to 4 km were less than 0.4 m and probably within the uncertainty generated by interpolation of the historical bathymetry and by changes in water level. According to Kunitsky (1989), in 1983, water shallower than the thickness of the annual sea-ice cover extended out to around 150–200 m from the shore, corresponding to the extent of the BFI zone which is separated from land-fast ice by cracks in sea ice. The intertidal zone exposed at low water levels and submerged at high-water levels resulted in a foreshore zone width of up to 180 m, where sea ice freezes to the bottom and isolated pockets of saline water up to 41‰ may collect (Kunitsky, 1989). Along the drilling profile, the unfrozen sediment layer increased in thickness from this border towards the sea, while landwards and in sand bars a seasonally frozen layer developed (Fig. 3, upper profile). In 2011, the mean depth along the entire profile was 2.76 m (Fig. 3, lower profile).

4.2 Water temperature and resistivity

Benthic water electrical conductivity and temperature measured between September 2008 and September 2009 in 7.2 m water depth directly before the east coast of the northern end of the island (Günther et al., 2013) varied strongly seasonally (Figs. 4a and 5). Bottom water temperature dropped from over 8°C on 1 September to negative temperatures by 16 October 2008. During most of this period, bottom water resistivity also fell, from peak values of $35 \Omega\text{m}$ to less than $2 \Omega\text{m}$. At the end of the period of observation, from 28 July until the end of August in 2009, variations in temperature and resistivity fell within a similar range of values. After the late summer cooling period, from mid-October until the beginning of July, temperatures are below -0.8°C and resistivity is below $3 \Omega\text{m}$. In June, bottom water began to freshen at temperatures below -1°C , eventually reaching summer values. In the early summer, following breakup of

the sea ice, high resistivity ($> 15 \Omega\text{m}$) bottom water varied in temperature, reaching peak values of 12°C .

Beneath the sea ice, from the end of October until after mid-May, bottom water electrical resistivity was below $1.7 \Omega\text{m}$ (i. e. above a conductivity of 6mS cm^{-1}), whereas the influence of the Lena River discharge increased this value up to over $10 \Omega\text{m}$ (corresponding to electrical conductivity below 1mS cm^{-1}) for the early summer (June). In July, the freshwater at the sea bed warmed to over 10°C . Winter resistivity varied less than $0.5 \Omega\text{m}$, whereas open-water season resistivity (July to mid-October) varied between 0.1 and $30 \Omega\text{m}$. The mean annual bottom water temperature was 2.1°C , and the mean annual bottom water resistivity was $10 \Omega\text{m}$ (corresponding to electrical conductivity of 0.09mS cm^{-1}).

4.3 Permafrost properties

The permafrost of Muostakh Island belongs to late Pleistocene IC deposits that accumulated in the region between at least 46.8 and 19.5kaBP based on radiocarbon ages (Schirrmeister et al., 2011a). It is overlain by a Holocene peat cover (Fig. 3). The IC is characterized by the occurrence of huge syngenetic ice wedges embedded in ice-rich silts and sands, peat horizons, and a considerable overall amount of organic carbon (total organic carbon content of up to 5% by weight; Schirrmeister et al., 2011a; Strauss et al., 2013). The oldest IC deposits lie up to 10m below modern sea level at Muostakh Island and are underlain by silts, sands and gravels interpreted as fluvial deposits of Pliocene to Early Pleistocene age (Fig. 3; Slagoda, 2004). In the following analysis, we report borehole observations and geoelectric surveys with reference to depths or elevations relative to sea level. Since sea-level changes over time, these results are not directly comparable. However, tidal variations around Tiksi are generally less than 10cm , although storm surges can lead to larger changes in sea level, up to $\pm 0.60 \text{m}$. The net change in mean annual sea level recorded three times per month at the Tiksi tide gauge between May 1983 and August 2011 was

3753

0.12m (data from Arctic and Antarctic Research Institute, St. Petersburg, accessed at www.whoi.edu/science/po/arcticsealevel/laptev.html on 16 March 2015).

Borehole temperatures are available for the cores 101, 304 and 305 obtained after drilling in May 1982 (101) and June 1983 (Fig. 4b; Kunitsky, 1989). The on-shore core 101 shows the cold-temperature regime of terrestrial permafrost with almost stable ground temperatures of about -9°C at the time of measurement that decrease slightly due to the seasonal winter signal in the upper 10m of the sediment (Fig. 4b). Both offshore cores 304 and 305 have temperatures that increase upwards from about -2°C at the borehole bottoms to 0°C at the sediment surface. Saline sea water lowers the pore water freezing temperature and decreases the resistivity in the upper part of the profile (Fig. 4b). The boundary between IBP and ice-free (unfrozen) permafrost lay at a depth of 8.3mb.s.l. in core 304 and 16mb.s.l. in core no 305. No boundary was encountered in core 101, which was frozen throughout. The IBP in the offshore boreholes was up to 7°C warmer than temperatures measured in borehole 101 at the shoreline.

4.4 Profiles of electrical resistivity and bathymetry

The results from three surveys conducted between 21 and 24 August 2011 are presented here. Two profiles of 1.5km length perpendicular to the eastern and western coasts of the northern cape of Muostakh Island, as well as one longer profile (4km) along the borehole profile drilled 28 years earlier (Figs. 1, 3 and 6; borehole 101 was drilled 29 years before surveying). Inverted bulk-sediment resistivities reached maximum values of $182 \Omega\text{m}$ for the western profile, $180 \Omega\text{m}$ for the drilling profile and $1300 \Omega\text{m}$ for eastern profile. The depth to IBP in 2011 was greater at each point along the drilling profile than observed in 1983. The IBP depths at the locations of cores 101, 304 and 305 were $5.2 \pm 0.6 \text{mb.s.l.}$, $10.9 \pm 3.6 \text{mb.s.l.}$ and $18.7 \pm 0.7 \text{mb.s.l.}$ determined using geoelectric soundings in 2011 (Fig. 3). Based on these values, the top of the IBP degraded 5.2 ± 0.6 , 2.6 ± 3.6 and $2.7 \pm 0.7 \text{m}$ at mean rates of 0.18 , 0.09 and 0.10ma^{-1} at each borehole location, respectively.

3754

For geoelectric soundings within the 1951 coastline, we linearly interpolated coastline positions from remote sensing imagery to geoelectric sounding position to estimate the period of inundation at each sounding. Figure 7 shows inferred mean submarine permafrost degradation rates since inundation as a function of these periods for soundings along the drilling profile and eastern profile. Since no interim determinations of IBP table depth were made since inundation, these degradation rates are mean rates for the entire 28 year period from first inundation until 2011. Instantaneous rates of degradation at or nearer to the shore line are probably higher. Results indicate that mean submarine permafrost degradation may be as rapid as 0.4 ma^{-1} for the initial decade, and that rates decrease over time, reaching a mean value of around 0.1 ma^{-1} sixty years after inundation. Assuming that the long-term erosion rate at the northern cape represents the mean rate since inundation, we can infer the duration of degradation for the borehole locations. In this case, the periods of inundation for boreholes 101, 304 and 305 were about 28, 112 and 253 years, respectively (Fig. 7).

5 Discussion

As coastal retreat progresses, the rate of IBP degradation slows (Hutter and Straughan, 1999). Are (2003) suggests using the distance from shoreline to approximate a time scale of inundation. Following this approach, the time of submergence at any point along the geoelectric profiles can be calculated based on the assumption that past erosion rates are similar to the long term mean rates observed over the past sixty years. The decrease in degradation rate with prolonged period since inundation is visible in our geoelectric profiles as a steeper inclination of the IBP table closer to shore (Fig. 6). The length of inundation of points distal to the island are approximately 260 years on the eastern profile, and closer to 3500 years of erosion on the western profile (based on profile length of 1700 m and coastal retreat rates of 0.5 and 6.5 ma^{-1} , respectively). Using the positions of the geoelectrical soundings for which date of inundation can be inferred, there is a decrease in the rate of degradation over time (Fig. 7). Nixon (1986)

3755

models a mean degradation rate of 0.1 ma^{-1} after 50 years of degradation for sediments with a freezing point of -1.8°C , matching the observations from the geoelectrical soundings shown in Fig. 3. Over the long term, Nixon's 1986 model and our results show a decrease in degradation rate to levels less than 0.1 ma^{-1} , as the thermal and solute concentration gradients between the sea floor and the IBP table become less and less steep, decreasing fluxes of heat and salt, respectively.

Studies in Siberia and Alaska have shown that submarine permafrost degradation is most rapid following inundation, when the thickness of the unfrozen sediment layer overlying the IBP is small, and thermal and diffusion gradients are steepest (Are, 2003; Harrison, 1982). Figure 7 shows a reduction in degradation rate as the length of inundation increases. The permafrost temperatures reported by Slagoda (1993) show warming of permafrost by almost 9°C within the first 100 years of inundation (Fig. 4b), up to the freezing temperature of the pore space solution. Based on 4 year coastal erosion rates, Molochushkin (1978) estimates that warming of the permafrost off the eastern shore of Muostakh Island occurs at 0.4°C a^{-1} over the first 10 years, but at an average rate of $0.25^\circ\text{C a}^{-1}$ for the first 30 years at a depth of 10 m below the sea floor.

Muostakh Island was chosen as a site for studying submarine permafrost degradation because its coastal retreat rate varies widely within a small area, over which larger scale drivers, such as air temperature, sea ice cover and storm events, can be assumed to be similar. Obvious differences between the eastern and western coasts include the orientation of the coastline, the potential maximum fetch before each coast, and the relative influence of riverine water and alongshore currents. Mean coastal retreat rates on the western and eastern shores of the island have differed by a factor of 13 for the past decades. Along both shores, thermo-abrasion of the submarine shoreface results in offshore transport of sediment, creating a concave submarine profile shape from the waterline out to about 1 km from shore. In contrast, mean water depth along the drilling profile was more than 2.5 m based on bathymetry measured during geoelectric surveying, throughout the profile. Although we could find no local sea ice thickness data for Muostakh Island, this exceeds probable maximum sea ice

3756

thickness. Ice thickness of 2.1 m was observed within 1 km of shore on the eastern shore of Buor Khaya Bay at the end of winter in 2012 (Günther et al., 2013). Sediment is thermo-abraded and deposited here in roughly equal measure. Differences in IBP depth along this profile are the result of differences in the duration and/or rate of IBP degradation. Differences between the western and eastern shores may be the result not only of differing IBP degradation rates and inundation periods but also of sediment budgets. Molochushkin (1978) attributes the thicker unfrozen sediment on the western side of Muostakh Island to the accumulation of marine sediment on flooded whereas erosion of sediment determines the depth to the IBP off the eastern shoreline. The similarity of the shoreface profiles suggests that this explanation is not sufficient to explain differences in IBP table inclination, however. Molochushkin and Gavrivev (1982) also presents interstitial salinity profiles for two cores from positions northeast of Muostakh Island (mean TDS $6.4 \text{ g (100 g)}^{-1}$; $2.6 \Omega \text{ m}$) and west of Muostakh (mean TDS of $1.8 \text{ g (100 g)}^{-1}$; $< 0.1 \Omega \text{ m}$) suggesting diffusion of seawater into the sediment rather than deposition under marine conditions.

The shape of the IBP table along the drilling profile is more complicated and may have depended on the shape of the northern cape over time. A distance 2.5 km from the 1983 coastline (core 305, Fig. 3) has probably been submerged for at least 250 years based on the mean erosion rate of 10 m a^{-1} for the period of record. Along the drilling profile, 645 m of the geoelectric profile have been inundated since drilling took place in 1982 and 1983 (Fig. 3). In Fig. 3, the position of the IBP table is interpolated linearly between borehole sites. In the geoelectric profile (Fig. 3), its position relative to sea level is determined at soundings spaced between 2 and 5 m apart along the entire profile. IBP table position based on geoelectric soundings therefore shows more detail than the borehole profile. It shows a pronounced dip of over 7 m (from 8.5 to 15.6 m b.s.l.) between the locations of boreholes 301 and 303, suggesting that the IBP there thawed more rapidly over the previous 28 years than locations closer to or further from shore. The slight rise in IBP beyond this dip corresponds to locally shallow parts of the 1983 bathymetry, where a sand bar resulted in water depth less than 1.5 m and

3757

where BFI probably formed each winter, allowing seasonal freezing of the sea floor (Kunitsky, 1989, borehole 303; also shown for Muostakh Island in Are, 2003). Although bathymetry can vary throughout the season and between years, the presence of BFI at least at the time of drilling may have led to cooling of the sediment and relative slowing of degradation locally (Osterkamp et al., 1989; Sellmann et al., 1992).

BFI acts as a thermal couple between the seabed and the atmosphere in winter, due to the higher thermal conductivity of ice compared to seawater. This effect tends to delay permafrost degradation immediately after inundation, until bathymetry exceeds the maximum depth of winter sea ice thickness of around 2 m, and the sea bed is covered by bottom water throughout the year (Osterkamp, 2001). Therefore, our observation of shallower IBP in places of former sand bars suggest that submarine permafrost preservation through thermal coupling of BFI outpaces the degradation effect associated with elevated brine concentration and injection under BFI. The duration of degradation on the abscissa in Fig. 7 includes any periods of BFI formation, and can therefore include a period of initial retardation of degradation. Beyond the depth of BFI, there are three distinct periods in the variation of benthic temperature and resistivity (Fig. 5): the winter sea ice period, a fluvially dominated period in early summer and a cooling phase in late summer. In the fall, the effect of sea ice formation is evident in the cooling and decreasing resistivity of the bottom water, as a result of higher salt contents. Beneath the winter ice, water temperatures are at the freezing point between -0.5 and -1.4 °C. Molochushkin (1978) reports mean annual seawater temperatures at Muostakh of 0.2 – 0.3 °C and resistivities of $10 \Omega \text{ m}$. Although the frequency and depth of measurements are not reported, these values are cooler than the 2.1 °C observed in this study but have the same mean salinity.

Differences in IBP depth between the eastern and western profiles may be the result of factors not observed in this study. For example, there may be systematic differences in benthic temperature and resistivity regimes on either side of Muostakh Island. We expect the sheltered western side to be less affected by the outflow of the Lena River on the eastern side, whereas we expect greater mixing and re-suspension due to

3758

5 wave action on the eastern side, especially when winds are from the N to NNE, and/or fetch exceeds 100 km. Such differences change boundary conditions for submarine permafrost and affect degradation rate. Nonetheless, the differences in IBP depth and inclination observed on either side of the island are at least consistent with differences in relative erosion rates even if permafrost degradation rates are assumed to be similar.

Our results indicate that permafrost degradation rates at Muostakh Island are consistent with those inferred for near-shore sites elsewhere on the Siberian shelf (Overduin et al., 2007, 2015). Since we calculate a decrease in submarine permafrost degradation rate with increased duration of inundation, most of the Siberian shelf region, which has been inundated for longer periods, probably has lower rates than those observed here, near the coastline. The degradation rates that we infer for Muostakh Island are probably typical for permafrost near the coast and the sea floor, where vertical thermal and solute concentration gradients within the sediment are steeper than for most of the shelf region. Following inundation, ice content decreases throughout submarine permafrost due to warming and the consequent thaw of pore ice. Nicolsky et al. (2012) shows this as an increase in water content based on assumed freezing characteristic curves. In this model, the rate of ice thaw depends on a suite of conditions during and antecedent to inundation. However, at 74.5° N, 118° E, for example, the depth of permafrost saturated to at least 50 % by ice degrades from about 25 to 200 mbsf, a mean rate of just below 0.01 m a⁻¹ (Nicolsky et al., 2012). Romanovskii and Hubberten (2001) show even lower rates of degradation of ice-bonded permafrost (defined as liquid water contents of < 5 % by weight). Such slow rates of degradation make it difficult to detect changes in IBP depth. Further difficulties result from high uncertainties associated with geophysical techniques. As we observed, short-term changes in sea level and sediment dynamics can also create problems for comparing measurements made on multi-year time scales.

The rate of coastal retreat influences the inclination of the IBP within the sediment. The IBP table inclinations along the three georesistivity profiles are consistent with a relationship between coastal retreat rate and the inclination of the IBP table. If erosion

3759

is rapid, the IBP table will tend to lie closer to the sediment surface (Fig. 8a; eastern profile). In cases where the coastal retreat rate is slow and permafrost degradation occurs, the inclination of the ice-bearing permafrost table will tend to be steeper (Fig. 8b; western profile). Thus, the duration of inundation and distance from the coastline are linked by the rate of coastline retreat, which is variable in time.

Observations of the inclination of the IBP table perpendicular to the coast in the Laptev and East Siberian seas show a high degree of spatial variability (Overduin et al., 2007), probably reflecting the temporally varying intensity of the processes described (Fig. 8c). Observing submarine permafrost depends on direct observation by drilling, sampling and temperature measurements (Fartyshev, 1993; Rachold et al., 2007) coupled with indirect observation using geophysical methods sensitive to property changes between frozen and unfrozen sediment. Since the coastal zone is highly dynamic, especially during spring melt and fall freeze-up, the logistics of measurements and continuous monitoring are difficult, requiring innovative new instrumentation and platforms for use in shallow water.

6 Conclusions

Offshore Soviet borehole data from 1982–1983 near the coast of Muostakh Island shows warming, salinization and increasing depth to ice-bonded submarine permafrost (IBP) with increasing distance from shore. Geoelectric surveys along the borehole profile 28 years later show that land has been inundated as a result of coastal erosion and suggest that the submarine permafrost created has degraded at mean rates of between 0.6 and 0.1 m a⁻¹ over decades to centuries. Based on comparison of two geoelectric profiles at an eroding and a stable stretch of coast, we suggest that, other factors being equal, greater rates of coastal erosion generally lead to a shallower inclination of the IBP table close to shore. These results show that IBP degrades most rapidly immediately after it is inundated year-round, and that degradation rates slow over time. On this basis, it is likely that degradation rates for most of the Siberian shelf permafrost are

3760

less than 0.1 m a^{-1} . Combined geophysical surveys and drilling are required to better study the salt water diffusion into the permafrost after inundation.

Acknowledgements. This work was funded by a Helmholtz Association of Research Centres (HGF) Joint Russian-German Research Group (HGF JRG 100). SPOT imagery were provided by SPOT Planet Action – an Astrium GEO initiative (project: Coastal erosion in East Siberia). Invaluable logistical support was provided by the Russian Hydrogeological Service in Tiksi, the Lena Delta Reserve and Waldemar Schneider.

References

- Are, F. E.: Thermal abrasion of sea coasts, *Polar Geogr. Geol.*, 12, 1–86, doi:10.1080/10889378809377343, 1988. 3749
- Are, F. E.: Shoreface of the Arctic seas – a natural laboratory for subsea permafrost dynamics, in: Proceedings of the Eighth International Conference on Permafrost, Zürich, Switzerland, edited by: Philips, M., Springman, S. M., and Arenson, L. U., Swets & Zeitlinger, Lisse, 21–25 July 2003, 27–32, 2003. 3745, 3755, 3756, 3758
- Barnes, D. F.: Geophysical methods for delineating permafrost, in: Proceedings of the International Conference on Permafrost, Lafayette, Indiana, 11–15 November 1963, edited by: Woods, K. B. and Alter, A. J., National Academy of Sciences, Washington, DC, 349–355, 1963. 3744
- Barnhart, K. R., Overeem, I., and Anderson, R. S.: The effect of changing sea ice on the physical vulnerability of Arctic coasts, *The Cryosphere*, 8, 1777–1799, doi:10.5194/tc-8-1777-2014, 2014. 3746
- Bauch, H. A., Mueller-Lupp, T., Taldenkova, E., Spielhagen, R. F., Kassens, H., Grootes, P. M., Thiede, J., Heinemeier, J., and Petryashov, V. V.: Chronology of the Holocene transgression at the North Siberian margin, *Global Planet. Change*, 31, 125–139, doi:10.1016/S0921-8181(01)00116-3, 2001. 3743
- Boike, J., Kattenstroth, B., Abramova, K., Bornemann, N., Chetverova, A., Fedorova, I., Fröh, K., Grigoriev, M., Grüber, M., Kutzbach, L., Langer, M., Minke, M., Muster, S., Piel, K., Pfeiffer, E.-M., Stoof, G., Westermann, S., Wischnewski, K., Wille, C., and Hubberten, H.-W.: Baseline characteristics of climate, permafrost and land cover from a new permafrost observatory in
3761
- the Lena River Delta, Siberia (1998–2011), *Biogeosciences*, 10, 2105–2128, doi:10.5194/bg-10-2105-2013, 2013. 3746
- Brown, J., Ferrians, O. J. J., Heginbottom, J. A., and Melnikov, E. S. (Eds.): Circum-Arctic map of permafrost and ground-ice conditions, Circum-Pacific Map Series CP-45, U.S. Geological Survey in Cooperation with the Circum-Pacific Council for Energy and Mineral Resources, Washington, DC, available at: <http://nsidc.org/data/ggd318.html> (last access: 15 June 2015), 2001. 3743
- Constable, S.: Ten years of marine CSEM for hydrocarbon exploration, *Geophysics*, 75, 75A67–75A81, 2010. 3744
- Corwin, R. F.: Marine permafrost detection using galvanic electrical resistivity methods, in: Off-shore Technology Conference, Houston, Texas, 2–5 May, 329–336, doi:10.4043/4480-MS, 1983. 3744
- Dallimore, S. R. and Collett, T. S.: Intrapermafrost gas hydrates from a deep core hole in the Mackenzie Delta, Northwest Territories, Canada, *Geology*, 23, 527–530, 1995. 3743
- Dmitrenko, I. A., Kirillov, S. A., Tremblay, L. B., Kassens, H., Anisimov, O. A., Lavrov, S. A., Razumov, S. O., and Grigoriev, M. N.: Recent changes in shelf hydrography in the Siberian Arctic: potential for subsea permafrost instability, *J. Geophys. Res.-Oceans*, 116, C10027, doi:10.1029/2011JC007218, 2011. 3743
- Fartyshev, A. I.: Osobennosti priberezhno-shelfovoi kriolitozony morya Laptevykh (Characteristics of the near-shore Laptev Sea shelf), Russian Academy of Sciences, Siberian Branch, Nauka, Novosibirsk, 1993 (in Russian). 3760
- Fedorova, I., Chetverova, A., Bolshiyarov, D., Makarov, A., Boike, J., Heim, B., Morgenstern, A., Overduin, P. P., Wegner, C., Kashina, V., Eulenburg, A., Dobrotina, E., and Sidorina, I.: Lena Delta hydrology and geochemistry: long-term hydrological data and recent field observations, *Biogeosciences*, 12, 345–363, doi:10.5194/bg-12-345-2015, 2015. 3746
- Frolov, A. D.: Electric and Elastic Properties of Frozen Earth Materials, ONTI PNC Russian Academy of Science Press, Pushchino, 1998. 3749
- Grigoriev, M. N.: Kriomorphogenez i litodinamika priberezhno-shelfovoi zony morei Vostochnoi Sibiri (Cryomorphogenesis and lithodynamics of the East Siberian near-shore shelf zone), Habilitation thesis, Mel’nikov Permafrost Institute, Russian Academy of Sciences, Siberian Branch, Yakutsk, 2008. 3743
- Grigoriev, M. N., Kunitsky, V. V., Chzhan, R. V., and Shepelev, V. V.: On the variation in geocryological, landscape and hydrological conditions in the Arctic zone of
3762

- East Siberia in connection with climate warming, *Geogr. Natural Resour.*, 30, 101–106, doi:10.1016/j.gnr.2009.06.002, 2009. 3745, 3746, 3751, 3769
- Günther, F., Overduin, P. P., Makarov, A. S., and Grigoriev, M. N. (Eds.): Russian-German Cooperation SYSTEM LAPTEV SEA: the Expeditions Laptev Sea – Mamontov Klyk 2011 & Buor Khaya 2012, vol. 664 of *Berichte zur Polar- und Meeresforschung (Reports on Polar and Marine Research)*, Alfred Wegener Institute, Bremerhaven, available at: <http://hdl.handle.net/10013/epic.41834> (last access: 15 June 2015), 2013. 3746, 3752, 3757
- Günther, F., Overduin, P. P., Yakshina, I. A., Opel, T., Baranskaya, A. V., and Grigoriev, M. N.: Observing Muostakh disappear: permafrost thaw subsidence and erosion of a ground-ice-rich island in response to arctic summer warming and sea ice reduction, *The Cryosphere*, 9, 151–178, doi:10.5194/tc-9-151-2015, 2015. 3745, 3746, 3749, 3750, 3751
- Harrison, W. D.: Formulation of a model for pore water convection in thawing subsea permafrost, *Mit. Ver. Was.*, 57, 3–24, 1982. 3744, 3756
- Hutter, K. and Straughan, B.: Models for convection in thawing porous media in support for the subsea permafrost equations, *J. Geophys. Res.-Sol. Ea.*, 104, 29249–29260, doi:10.1029/1999JB900288, 1999. 3755
- Kang, M. and Lee, J. S.: Evaluation of the freezing-thawing effect in sand-silt mixtures using elastic waves and electrical resistivity, *Cold Reg. Sci. Technol.*, 113, 1–11, doi:10.1016/j.coldregions.2015.02.004, 2015. 3749
- King, M. S., Zimmerman, R. W., and Corwin, R. F.: Seismic and electrical properties of unconsolidated permafrost, *Geophys. Prospect.*, 36, 349–364, 1988. 3749
- Kunitsky, V. V.: *Kriolitologiya Nizovya Leny (Cryolithology of the Lower Lena)*, Melnikov Permafrost Institute, Russian Academy of Sciences, Siberian Branch, Yakutsk, 1989 (in Russian). 3747, 3751, 3752, 3754, 3758, 3767
- Lachenbruch, A. H.: Thermal effects of the ocean on permafrost, *Bull. Geol. Soc. Am.*, 68, 1515–1530, 1957. 3743
- McGuire, A. D., Anderson, L. G., Christensen, T. R., Dallimore, S., Guo, L., Hayes, D. J., Heimann, M., Lorenson, T. D., Macdonald, R. W., and Roulet, N.: Sensitivity of the carbon cycle in the Arctic to climate change, *Ecol. Monogr.*, 79, 523–555, doi:10.1890/08-2025.1, 2009. 3743
- Molochushkin, E. N.: The effect of thermal abrasion on the temperature of the permafrost in the coastal zone of the Laptev Sea, in: *Proceedings of the Second International Conference on Permafrost*, Yakutsk, U.S.S.R., 1973, 13–28 July, edited by: Sanger, F. J. and Hyde, P. J., vol.

3763

- USSR Contributions, National Academy of Sciences, Washington, DC, 90–93, 1978. 3756, 3757, 3758
- Molochushkin, E. N. and Gavriev, R. I.: Structure, phase composition and heat regime of the bottom of the coastal Laptev Sea, in: *The Arctic Ocean and Its Coast in the Cenozoic Era (Severnyi Ledovityi Okean i Ego Poberezh'e v Kainozoe)*, edited by: Tolmachev, A. I., Amerind Publishing Co. Pvt. Ltd., New Delhi, p. 564, 1982. 3757
- Nicolosky, D. J., Romanovsky, V. E., Romanovskii, N. N., Kholodov, A. L., Shakhova, N. E., and Semiletov, I. P.: Modeling sub-sea permafrost in the East Siberian Arctic Shelf: the Laptev Sea region, *J. Geophys. Res.-Earth*, 117, F03028, doi:10.1029/2012JF002358, 2012. 3759
- Nixon, J. F.: Thermal simulation of subsea saline permafrost, *Can. J. Earth Sci.*, 23, 2039–2046, doi:10.1139/e86-188, 1986. 3755, 3756
- Osterkamp, T. E.: Sub-sea permafrost, in: *Encyclopedia of Ocean Sciences*, edited by: Steele, J. H., Thorpe, S. A., and Turekian, K. K., vol. 5, Academic Press, New York, London, 2902–2912, 2001. 3758
- Osterkamp, T. E., Baker, G. C., Harrison, W. D., and Matava, T.: Characteristics of the active layer and shallow subsea permafrost, *J. Geophys. Res.-Oceans*, 94, 16227–16236, doi:10.1029/JC094iC11p16227, 1989. 3758
- Overduin, P. P., Hubberten, H.-W., Rachold, V., Romanovskii, N. N., Grigoriev, M. N., and Kasymkaya, M.: The evolution and degradation of coastal and offshore permafrost in the Laptev and East Siberian Seas during the last climatic cycle, in: *Coastline Changes: Interrelation of Climate and Geological Processes*, edited by: Harff, J., Hay, W., and Tetzlaff, D., vol. 426, The Geological Society of America Special Paper, Boulder, Colorado, USA, 97–111, doi:10.1130/2007.2426(07), 2007. 3759, 3760
- Overduin, P. P., Westermann, S., Yoshikawa, K., Haberlau, T., Romanovsky, V., and Wetterich, S.: Geoelectric observations of the degradation of nearshore submarine permafrost at Barrow (Alaskan Beaufort Sea), *J. Geophys. Res.-Earth*, 117, F02004, doi:10.1029/2011JF002088, 2012. 3744, 3749
- Overduin, P. P., Liebner, S., Knoblauch, C., Günther, F., Wetterich, S., Schirrmeister, L., Hubberten, H.-W., and Grigoriev, M. N.: Methane oxidation following submarine permafrost degradation: measurements from a Central Laptev Sea shelf borehole, *J. Geophys. Res.-Biogeo.* 120, 965–978, doi:10.1002/2014JG002862, 2015. 3743, 3759

3764

- Ping, C.-L., Michaelson, G. J., Guo, L., Jorgenson, M. T., Kanevskiy, M., Shur, Y., Dou, F., and Liang, J.: Soil carbon and material fluxes across the eroding Alaska Beaufort Sea coastline, *J. Geophys. Res.-Biogeo.*, 116, G02004, doi:10.1029/2010JG001588, 2011. 3746
- Rachold, V., Bolshiyarov, D. Y., Grigoriev, M. N., Hubberten, H.-W., Junker, R., Kunitsky, V. V., Merker, F., Overduin, P., and Schneider, W.: Nearshore arctic subsea permafrost in transition, *Eos T. Am. Geophys. Un.*, 88, 149–150, doi:10.1029/2007EO130001, 2007. 3760
- Romanovskii, N. N. and Hubberten, H.-W.: Results of permafrost modelling of the lowlands and shelf of the Laptev Sea region, Russia, *Permafrost Periglac.*, 12, 191–202, doi:10.1002/ppp.387, 2001. 3759
- Schirrmeister, L., Grosse, G., Wetterich, S., Overduin, P. P., Strauss, J., Schuur, E. A. G., and Hubberten, H.-W.: Fossil organic matter characteristics in permafrost deposits of the north-east Siberian Arctic, *J. Geophys. Res.-Biogeo.*, 116, G00M02, doi:10.1029/2011JG001647, 2011a. 3753
- Schirrmeister, L., Kunitsky, V., Grosse, G., Wetterich, S., Meyer, H., Schwamborn, G., Babiy, O., Derevyagin, A., and Siegert, C.: Sedimentary characteristics and origin of the Late Pleistocene Ice Complex on north-east Siberian Arctic coastal lowlands and islands – a review, *Quatern. Int.*, 241, 3–25, doi:10.1016/j.quaint.2010.04.004, 2011b. 3745
- Scott, W. J., Sellmann, P. V., and Hunter, J. A.: Geophysics in the study of permafrost, in: *Geotechnical and Environmental Geophysics*, edited by: Ward, S., Soc. of Expl. Geoph., Tulsa, 355–384, 1990. 3744
- Sellmann, P. V., Delaney, A. J., and Arcone, S. A.: Coastal Submarine Permafrost and Bedrock Observations Using DC Resistivity, vol. 89-13 of *U.S. Army Cold Regions Research and Engineering Laboratory (CRREL) Report*, National Technical Information Service, Hanover, New Hampshire, 1989. 3744
- Sellmann, P. V., Delaney, A. J., Chamberlain, E. J., and Dunton, K. H.: Seafloor temperature and conductivity data from Stefansson Sound, Alaska, *Cold Reg. Sci. Technol.*, 20, 271–288, doi:10.1016/0165-232X(92)90034-R, 1992. 3758
- Shakhova, N. and Semiletov, I.: Methane release and coastal environment in the East Siberian Arctic shelf, *J. Marine Syst.*, 66, 227–243, doi:10.1016/j.jmarsys.2006.06.006, 2007. 3743
- Slagoda, E. A.: Genesis i mikrostroenie kriolitogennykh otlozhenii Bykovskogo polyostrova i ostrova Muostakh (Genesis and microstructure of cryolithogenic deposits at the Bykovsky Peninsula and the Muostakh Island), PhD thesis, Mel'nikov Permafrost Institute, Russian Academy of Sciences, Siberian Branch, Yakutsk, 1993 (in Russian). 3747, 3756, 3767

3765

- Slagoda, E. A.: Kriolitogennye otlozheniya primorskoi ravniny morya Laptevykh: litologiya i mikromorfologiya (poluostrov Bykovskiy i ostrov Muostakh) – Cryolithogenic Sediments of the Laptev Sea Coastal Lowland: Lithology and Micromorphology (Bykovsky Peninsula and Muostakh Island), Ekspress, Tyumen, 2004 (in Russian). 3747, 3753, 3767, 3770
- Solomon, S. M., Taylor, A. E., and Stevens, C. W.: Nearshore Ground Temperatures, Seasonal Ice Bonding, and Permafrost Formation Within the Bottom-Fast Ice Zone, Mackenzie Delta, NWT, in: *Proceedings of the Ninth International Conference on Permafrost*, Fairbanks, Alaska, June 29–03 July, edited by: Kane, D. L. and Hinkel, K. M., vol. 2, 1675–1680, 2008. 3744
- Strauss, J., Schirrmeister, L., Grosse, G., Wetterich, S., Ulrich, M., Herzsuh, U., and Hubberten, H.-W.: The deep permafrost carbon pool of the Yedoma region in Siberia and Alaska, *Geophys. Res. Lett.*, 40, 6165–6170, doi:10.1002/2013GL058088, 2013. 3753

3766

Table 1. Borehole characteristics.

Borehole number ^a	Latitude, longitude	Water depth [m]	Borehole depth [m b.s.l.]	IBP ^b table depth [m b.s.l.]
101_82	71.6162° N, 129.926° E	0	52	0
301_83	71.6183° N, 129.9208° E	2.4	7.8	3.3
302_83	71.6188° N, 129.9190° E	3	10	4
303_83	71.6199° N, 129.9156° E	2	12	7
304_83	71.6217° N, 129.9083° E </td <td>3.4</td> <td>50.7</td> <td>8.3</td>	3.4	50.7	8.3
305_83	71.6254° N, 129.8958° E	3	54	16

^a data from Kunitzky (1989); Slagoda (1993, 2004); ^b IBP: ice-bonded permafrost.

3767

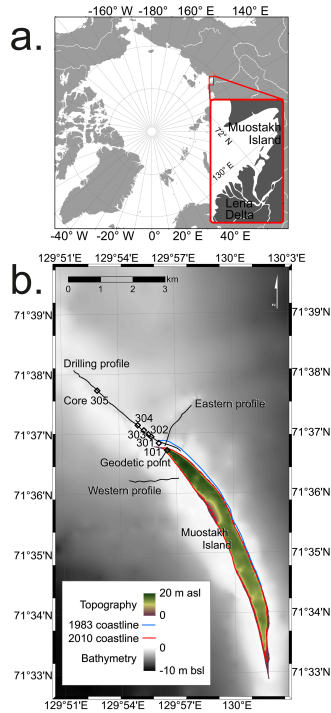


Figure 1. (a) The location of the study site in the central Laptev Sea, eastern Siberia, Russia. (b) The topography of Muostakh Island and the surrounding bathymetry. The reference geodetic point and borehole locations are shown as diamonds and the three geoelectric profiles as black lines. The blue line surrounding the island indicates the position of the coastline in 1983, the red line the coastline in 2010.

3768

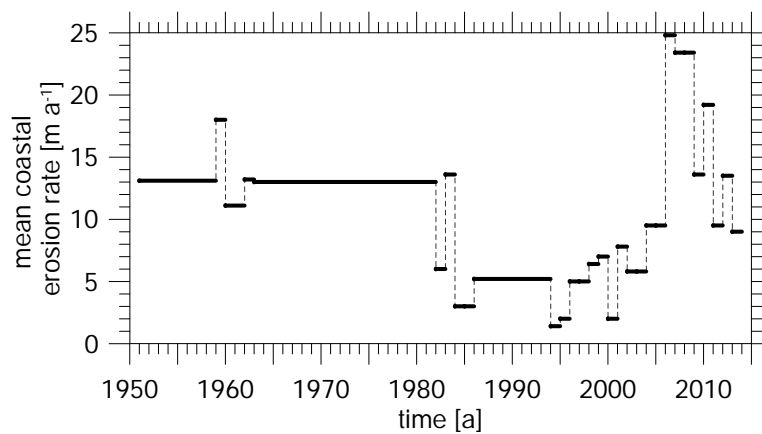


Figure 2. The mean annual erosion rate at the northern cape of Muostakh Island has been measured by determination of the position of the upper edge of the bluff relative to a geodetic point (measurements are indicated as mean values over a period) since 1951. The greater the absolute value, the higher the erosion rate (reproduced from Grigoriev et al., 2009 for data up to 2008).

3769

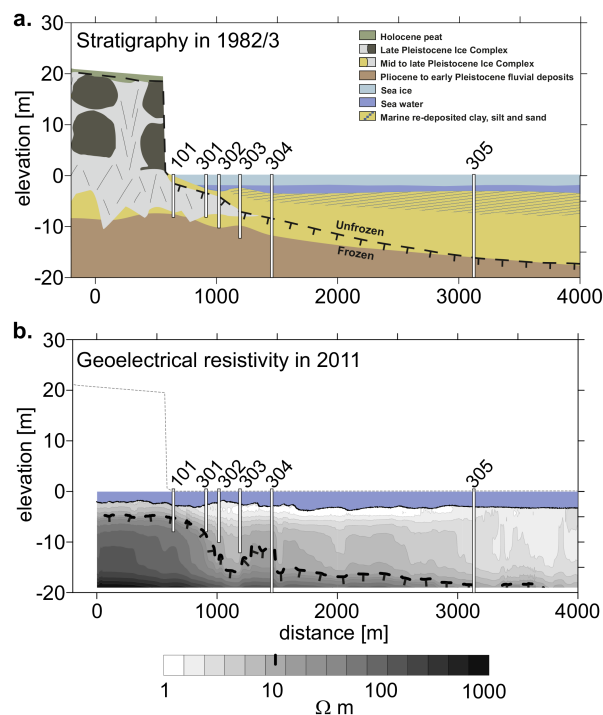


Figure 3. A comparison of the results of the drilling in 1982 and 1983 with the inverted resistivity in 2011. The stratigraphy in the upper figure is based on the coastal exposures and the interpolation of borehole sediment stratigraphy, redrawn from Slagoda (2004). The 15 Ω m isopleth is indicated with dashed lines on the resistivity cross-section. Vertical exaggeration is 37 times.

3770

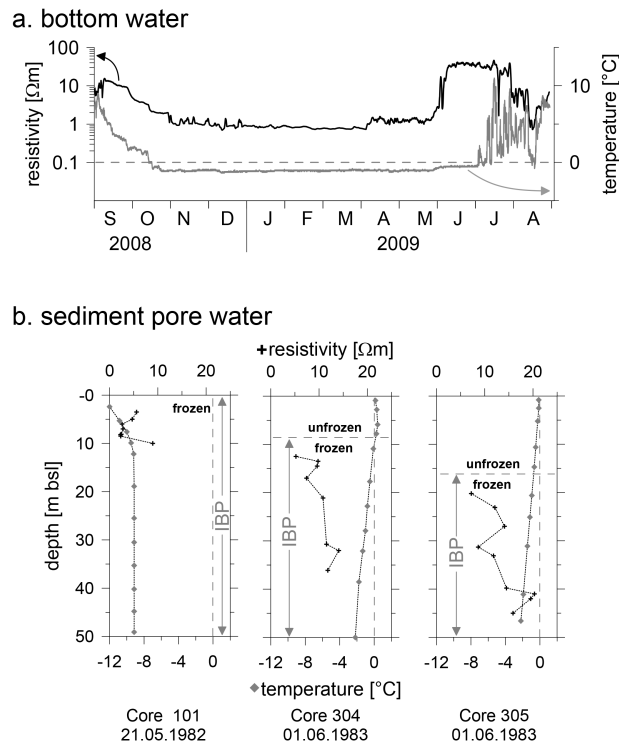


Figure 4. Water electrical resistivity and temperature are shown for: **(a)** bottom water measured for the period 1 September 2008 – 31 August 2009 in 7.2 m water depth and **(b)** for sediment pore water from cores recovered from boreholes 101, 304 and 305 on the dates indicated (Figs. 1 and 3; Table 1).

3771

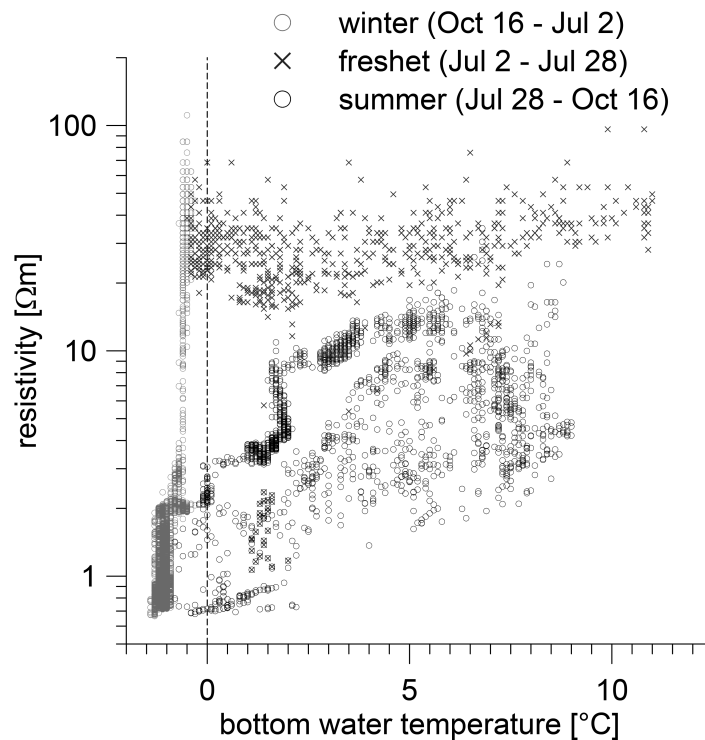


Figure 5. Bottom water resistivity plotted as a function of temperature for a one year period (1 September 2008–31 August 2009) in 7.2 m deep water northeast of Muostakh Island in the central Laptev Sea. Three periods are distinguished: winter ice covered, freshwater and late summer.

3772

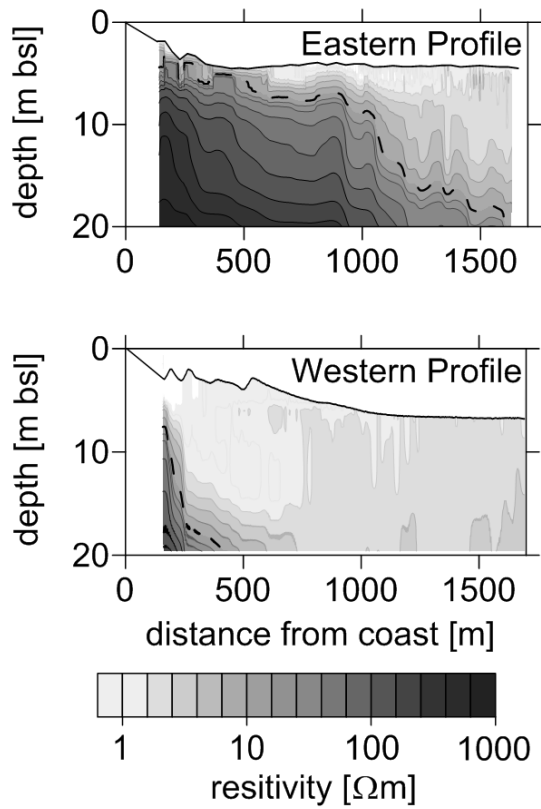


Figure 6. Inversions of the georesistivity of the eastern and western geoelectric profiles (positions shown in Fig. 1).

3773

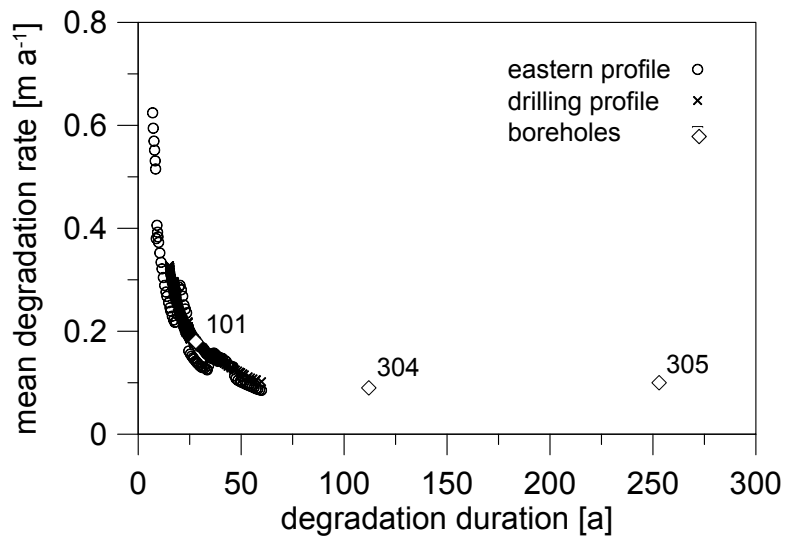


Figure 7. Permafrost degradation rate inferred from geoelectric sounding depth and position for the eastern and borehole geoelectric profiles and for three boreholes indicated by number (diamonds). Data are shown for soundings at locations flooded since 1951.

3774

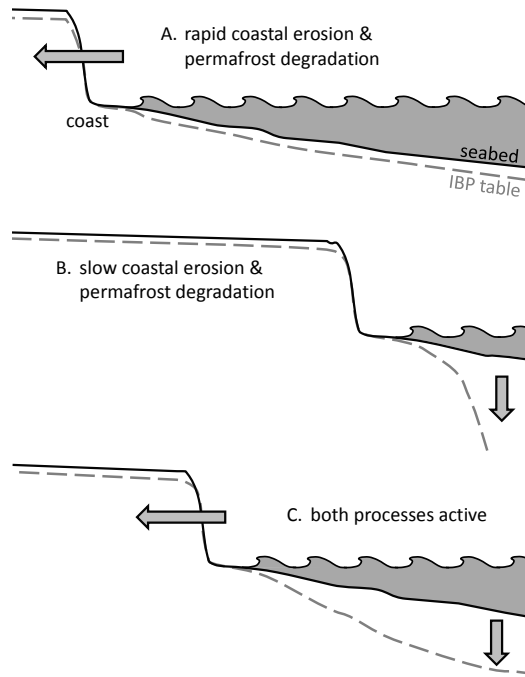


Figure 8. The relative rates of coastline retreat and permafrost degradation affect the shape of the ice-bonded permafrost (IBP) table beneath the shoreface profile sediment. In A., rapid coastline retreat lead to an IBP table close to the sediment surface; in B., a stable coastline leads to an IBP table that is more steeply inclined; in C., most IBP table inclinations can be expected to reflect a complicated suite of factors, including temporally variable coastline retreat, permafrost degradation rates, and near-shore sediment dynamics.